JACS
JOURNAL OF THE AMERICAN CHEMICAL SOCIETY

Article

pubs.acs.org/JACS

Retaining Glycosyltransferase Mechanism Studied by QM/MM Methods: Lipopolysaccharyl-α-1,4-galactosyltransferase C Transfers α-Galactose via an Oxocarbenium Ion-like Transition State

Hansel Gómez,[‡,†] Iakov Polyak,[§] Walter Thiel,[§] José M. Lluch,[‡,†] and Laura Masgrau*[,‡]

[‡]Institut de Biotecnologia i de Biomedicina and [†]Departament de Química, Universitat Autònoma de Barcelona, 08193 Bellaterra, Barcelona, Spain

[§]Max-Planck-Institut für Kohlenforschung, D-45470 Mülheim an der Ruhr, Germany

Supporting Information

ABSTRACT: Glycosyltransferases (GTs) catalyze the highly specific biosynthesis of glycosidic bonds and, as such, are important both as drug targets and for biotechnological purposes. Despite their broad interest, fundamental questions about their reaction mechanism remain to be answered, especially for those GTs that transfer the sugar with net retention of the configuration at the anomeric carbon (retaining glycosyltransferases, ret-GTs). In the present work, we focus on the reaction catalyzed by lipopolysaccharyl-α-1,4-galactosyltransferase C (LgtC) from *Neisseria meningitides*. We study and compare the different proposed mechanisms (S_Ni, S_Ni-like, and double displacement mechanism via a covalent glycosyl-enzyme intermediate, CGE) by using density functional theory (DFT) and quantum mechanics/molecular mechanics (QM/MM) calculations on the full enzyme. We characterize a dissociative single-displacement (S_Ni) mechanism consistent with the experimental data, in which the acceptor substrate attacks on the side of the UDP leaving group that acts as a catalytic base. We identify several key interactions that help this front-side attack by stabilizing the transition state. Among them, Gln189, the putative nucleophile in a double displacement mechanism, is shown to favor the charge development at the anomeric center by about 2 kcal/mol, compatible with experimental mutagenesis data. We predict that using 3-deoxylactose as acceptor would result in a reduction of k_{cat} to 0.6−3% of that for the unmodified substrates. The reactions of the Q189A and Q189E mutants have also been investigated. For Q189E, there is a change in mechanism since a CGE can be formed which, however, is not able to evolve to products. The current findings are discussed in the light of the available experimental data and compared with those for other ret-GTs.

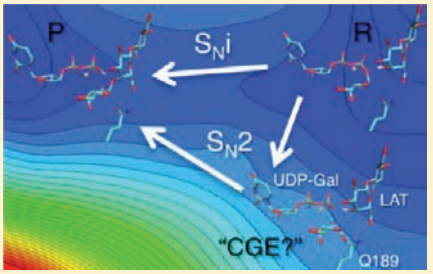

INTRODUCTION

Glycosyltransferases (GTs) are a large family of enzymes that catalyze the biosynthesis of glycosidic linkages by the stereo- and regiospecific transfer of monosaccharides from donors, typically nucleotide sugars, to a variety of acceptors (other saccharides, lipids, proteins, DNA).[1] GTs are responsible for the synthesis of biopolymers, therapeutically important glycosylated natural product antibiotics, and anticancer agents. Moreover, they are part of important biological pathways and are implicated in many diseases. Despite the relevance of their reactions and products in different fields, the understanding of their catalytic mechanism remains one of the fundamental challenges in glycoscience.[2−4] This is specially the case for retaining GTs, which catalyze the sugar transfer with net retention of the configuration at the anomeric carbon.

Neisseria meningitidis is a bacterium that lives within the nasopharyngeal tract of humans and can become a human-specific pathogen causing invasive, life-threatening infections, such as meningitis and septicemia.[5] Its great virulence is related to the presence of lipooligosaccharides (LOSs) on its cell surface that can mimic those of human glycolipids, thus, avoiding the recognition by the human immune system. Lipopolysaccharyl-α-1,4-galactosyltransferase C (EC 2.4.1.44, LgtC) from *N. meningitidis* (a member of family 8 of GTs)[6] plays a key role in the biosynthesis of the oligosaccharide part of LOS structures. Therefore, it represents a very attractive therapeutic target for new antibiotics.[7] This enzyme catalyzes the transfer of an α-galactose from uridine 5′-diphospho-α-galactose (UDP-Gal) to a galactose of the terminal lactose (LAT) on the bacterial LOS to yield an elongated oligosaccharide with an overall retention of stereochemistry at the anomeric carbon atom. Thus, LgtC can be classified as a retaining GT. Moreover, it presents a GT-A fold, one of the three folds reported for GTs, characterized by the presence in the active site of the Asp-X-Asp (DXD) signature implicated in the binding of the donor sugar substrate and/or the coordination of a divalent cation.[4]

Virtually all retaining glycosidases (GHs) utilize a double-displacement reaction mechanism. By analogy, catalysis by retaining GTs was initially believed to proceed in a similar way (Scheme 1A) with the formation and subsequent cleavage of a

Received: November 8, 2011
Published: February 21, 2012

ACS Publications © 2012 American Chemical Society

dx.doi.org/10.1021/ja210490f | J. Am. Chem. Soc. 2012, 134, 4743−4752

Scheme 1. Proposed Mechanisms for the Retaining GTs[a]

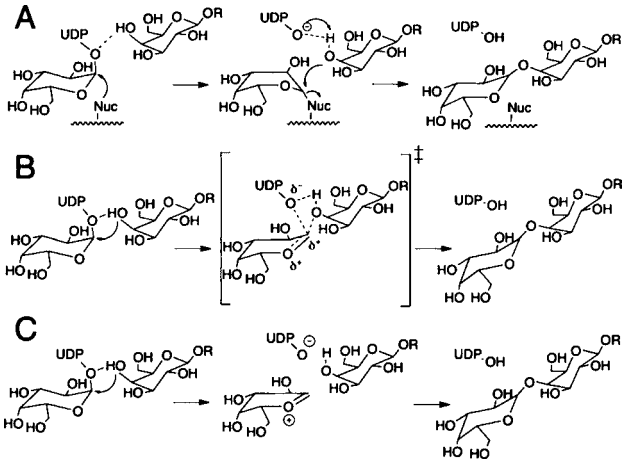

[a](A) Double-displacement mechanism with formation of a covalently bound glycosyl-enzyme intermediate. (B) Concerted front-side single displacement (S_Ni) with an oxocarbenium ion-like transition state. (C) S_Ni-like mechanism in which a short-lived oxocarbenium-phosphate ion pair intermediate is formed.

covalent glycosyl-enzyme (CGE) intermediate, which requires the existence of an appropriately positioned nucleophile within the active site.[3,4,8] However, conclusive evidence for the formation of CGE intermediates has been elusive for many years although several experiments point in that direction.[9−11]

The problem is even more challenging for those retaining GTs in which no good candidate for the catalytic nucleophile seems to exist within the active site. This is the case for LgtC from *N. meningitidis*, whose X-ray crystal structure was the first one determined for a glycosyltransferase in the form of a ternary complex with both donor and acceptor substrate analogues.[12] This 2.0 Å crystal structure contains the inert UDP-2′-deoxy-2′-fluoro-α-galactose (UDP-2′FGal) and the nonreactive 4-deoxylactose.[12] Quite surprisingly, the most suitably positioned active-site residue on the β-face of the donor sugar for a nucleophilic attack on the anomeric carbon is Gln189 (whose side chain oxygen atom is 3.5 Å away from the anomeric carbon). However, the nucleophilic character of the amide of Gln189 should be rather poor. Experimentally, both the Q189A and Q189E LgtC mutants display 3% residual transferase activity, indicating the limited relevance of Gln189 as catalytic nucleophile.[11,12]

An alternative mechanism involving retention of configuration at the anomeric carbon is the so-called S_Ni ("i" for "internal return") mechanism,[13] which occurs through a front-side attack of the nucleophile (the O4 atom of lactose) on the same side as the leaving group (UDP) forming an oxocarbenium ion-like transition state (Scheme 1B), or even an oxocarbenium-phosphate short-lived ion pair intermediate (Scheme 1C) in an S_Ni-like mechanism.[4] A front-side attack might seem unfavorable in view of the limited free space available in the active site of LgtC and the bulky nature of both the ingoing and the outgoing groups, but such steric problems could be alleviated by having a highly dissociative S_Ni transition state (Scheme 1B) or even a short-lived ion pair intermediate (Scheme 1C). Very recently, experimental work on trehalose-6-phosphate synthase (OtsA), a retaining GT of the GT20 family, has provided evidence for a dissociative mechanism with charge development at the anomeric center.[14,15]

Very little computational work has been devoted to the study of retaining GTs and, to the best of our knowledge, only one paper has been published about LgtC: Tvaroška[16] used density functional theory (DFT) methods to study a cluster model based on the crystallographic structure of LgtC. This reduced model contained 136 atoms, including those from five protein residues (three of them coordinating the Mg^{2+} cation). To mimic the positioning effect of the missing protein environment, the α-carbons of the five included amino acids were constrained to their crystallographic positions. Tvaroška predicted a one-step S_Ni mechanism with an energy barrier of 31.3 kcal/mol at the B3LYP/6-311++G**//B3LYP/6-31G* level of theory. Treating the environment as a dielectric continuum with dielectric constants of 2 (78) reduced this barrier by 7 (21) kcal/mol and thus led to rough estimates for the barrier in the range of 10−24 kcal/mol. However, the choice of a reduced cluster model neglects the effects of many important residues and interactions that are actually present in the enzyme−substrate complex, which causes uncertainties and prevents a true understanding of the role of the enzyme in driving the reaction (see Figure 1 for a view of all the enzyme−substrate interactions seen in the crystallographic structure).[12]

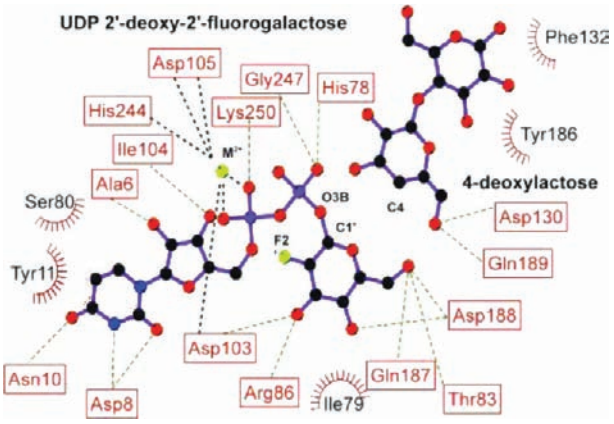

Figure 1. LIGPLOT[17] diagram of UDP-Gal and LAT analogues bound in the LgtC active site (PDB code: 1GA8). The metal coordination and hydrogen bonds between the substrates and the surrounding amino acids are represented by black or green dashed lines, respectively. Nonligand residues in hydrophobic contacts with the substrates are represented by red semicircles with radiating spokes.

In this paper, we present for the first time a full-enzyme hybrid quantum mechanical/molecular mechanical (QM/MM) study of the catalytic mechanism of a retaining glycosyltransferase with the GT-A fold, that is, LgtC from *N. meningitidis*. We explore the different mechanistic alternatives outlined above and analyze the role of the most relevant active-site residues and interactions that support the catalytic action of LgtC despite the absence of a good nucleophilic agent. In addition, we consider the effect of different mutations in the enzyme and of modifications in the substrates. Finally, a comparison with other retaining GTs is made, and possible relationships between specificity and mechanism are discussed.

While this paper was being written, a computational QM/MM study of OtsA was published[18] which concluded that OtsA reacts via an S_Ni-like mechanism with a very short-lived ion-pair intermediate. OtsA differs from LgtC in having the GT-B fold, which lacks the DXD signature and does not require a divalent metal for catalysis. Given these differences, it is unclear whether

to expect similar or different mechanistic behavior in LgtC and OtsA.

MODELS AND METHODS

Initial coordinates for the wild-type enzyme were taken from the X-ray structure[12] (PDB Code: 1GA8, resolution 2.0 Å). The protonation states of the titratable residues (His, Glu, Asp, Arg, Lys) were chosen based on the pK_a values given by the empirical PROPKA procedure[19] and verified through visual inspection. The substrate analogues present in the crystal structure (UDP 2-deoxy-2′-fluoro-galactose and 4-deoxylactose) were transformed manually into the original substrates, UDP-galactose (UDP-Gal) and lactose (LAT), respectively, while the manganese ion was modeled by Mg^{2+}. This latter choice was also made in the previous model study.[16] In the retaining glycosyltransferases with the GT-A fold, the M^{2+} ion is known to act as a Lewis acid that facilitates the departure of the leaving group,[4] and it is known that both Mn^{2+} and Mg^{2+} can adopt this role in a similar manner.[20] Generally, according to previous theoretical work, both cations behave remarkably similar and exhibit the same coordination preferences.[21] More specifically, both divalent ions have given almost the same results in a thorough validation study[22] of α-glycosidic bond dissociation in sugar phosphates derived from the crystal structure of LgtC; for example, the M05-2X energies (bond lengths) differ between the studied Mg^{2+} and Mn^{2+} complexes by less than 0.2 kcal/mol (0.01 Å). This has been taken as justification for using enzymatic models in which Mn^{2+} is replaced by a computationally more convenient Mg^{2+} cation.[22] Still, test calculations have been done for the most relevant pathways to ensure that this replacement is valid here (see below).

A partial solvation scheme was used to solvate the region of 24 Å around the anomeric center by overlaying a water sphere on the enzyme. The solvated system was first relaxed by performing energy minimizations at the MM level using the CHARMM22 force field[23−25] as implemented in the CHARMM program.[26,27] For the sugar moieties, the topology and parameters from the CHARMM force field for carbohydrates were used, including the recently released ones for glycosidic linkages between hexopyranoses.[28] The solute atoms were initially frozen for 10 000 conjugate gradient optimization steps. In the subsequent minimizations, the restraints on the protein and ligand atoms were gradually released. The prepared system (see Figure 2) contained 6728 atoms, including 755 TIP3P water molecules, and served as starting point for the QM/MM calculations.

The QM/MM calculations were done with the modular program package ChemShell[29] using TURBOMOLE,[30] Gaussian03[31] or MNDO2005[32] to obtain the QM energies and gradients at the DFT (BP86,[33−37] B3LYP[33−35,38−40] and M05-2X[41] functionals) or SCC-DFTB[42,43] levels, respectively. MM energies and gradients were evaluated by DL_POLY,[44] which was accessed through the ChemShell package, using the CHARMM force field. An electronic embedding scheme[45] was adopted in the QM/MM calculations with the MM point charges being incorporated into the one-electron Hamiltonian during the QM calculation. No cutoffs were introduced for the nonbonding MM and QM/MM interactions. Seven hydrogen link atoms were employed to treat the QM/MM boundary with the charge shift model.[46,47]

All residues and water molecules within 12 Å of the anomeric center were included in the optimization process (1225 atoms) as the active region while the remaining atoms were kept fixed. The QM region incorporated 101 atoms: those from the α and β galactose rings (from UDP-Gal and LAT, respectively), Mg^{2+} and its first coordination sphere (phosphate groups from UDP and the side chains of residues Asp103, Asp105 and His244), as well as the side chain of Gln189 (see Scheme 2). The total charge of the QM region was −2.

Reaction paths were scanned by performing constrained optimizations along properly defined reaction coordinates in steps of 0.2 Å. This provided starting structures for subsequent full optimization of all relevant stationary points, employing the low-memory Broyden-Fletcher-Goldfarb-Shanno (L-BFGS)[48,49] algorithm in the case of minimizations and the microiterative optimizer combining both the partitioned rational function optimizer (P-RFO)[50,51] and L-BFGS during the transition state search. All these algorithms are implemented in the HDLCopt[52] module of ChemShell. Frequency calculations on the QM region confirmed that all reported transition states are characterized by a single imaginary frequency and a suitable transition vector that corresponds to the investigated reaction. We ensured by intrinsic reaction coordinate (IRC) calculations and visual inspection of the optimized structures that the computed stationary points are connected by continuous pathways.

Geometry optimizations were generally carried out at the QM(BP86/SVP)/CHARMM level using the BP86 functional and the SVP[53] basis set in combination with the resolution-of-the-identity (RI) approximation.[54,55] For more accurate energy evaluations, we performed single-point energy calculations with other functionals and

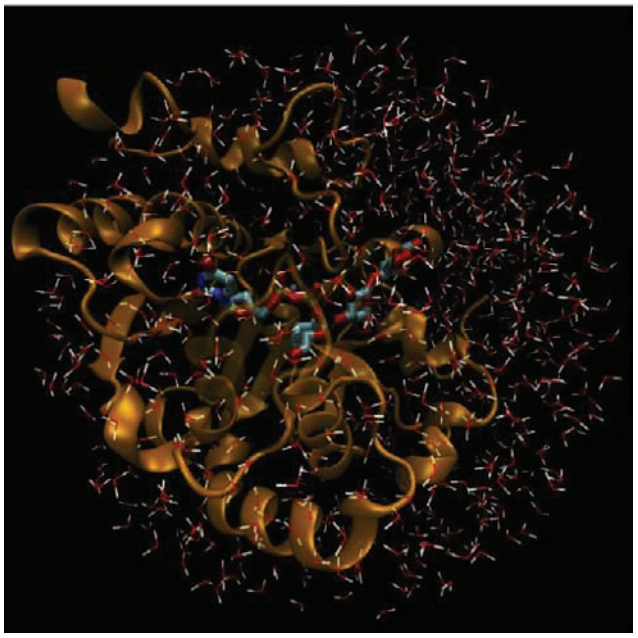

Figure 2. Representation of the system studied: UDP-Gal, LAT, and Mg^{2+} (sticks) bound to LgtC (orange cartoon) and solvated with a 24 Å radius sphere of water molecules.

Scheme 2. Active Site Representation Showing the QM/MM Partition Used in the Present Work[a]

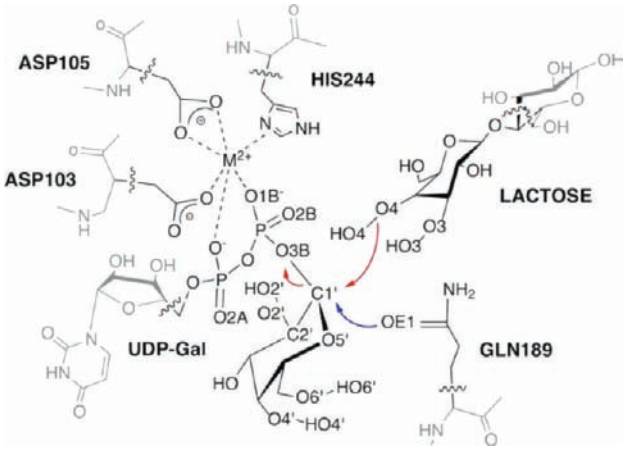

[a]QM (MM) atoms are depicted in black (grey). The boundary between the QM and MM regions is indicated by wavy lines. The first step of the double displacement mechanism and the front-side attack mechanism are illustrated by blue and red arrows, respectively. Atoms mentioned in the text are labeled.

dx.doi.org/10.1021/ja210490f | J. Am. Chem. Soc. 2012, 134, 4743−4752

larger basis sets: B3LYP, M05-2X, and DFT-D[56] methods; TZVP[57] and def2-TZVPP(d)[58] basis sets (see Supporting Information (SI) for more details). Natural population analysis (NPA)[59] charges were determined from QM/MM calculations with QM = B3LYP/TZVP and BP86/TZVP.

Umbrella sampling at the SCC-DFTB/CHARMM22 level was performed to compute the potential of mean force (PMF) and the free energy profile for the front-side mechanism using the dynamics module within ChemShell (see SI for more details).

The contribution of different residues to the QM/MM energy in the front-side attack mechanism was examined by setting their point charges to zero in additional energy calculations along the QM(BP86/SVP)/CHARMM reaction path. In the case of Gln189, extra QM/MM calculations were performed in which Gln189 was assigned the charges of a glutamate.

The Molefacture plugin for VMD[60] was used to generate the mutants of the enzyme and the modified substrates. This program also served to generate all the drawings showing molecular structures.

RESULTS AND DISCUSSION

Front-Side Attack (S_Ni or S_Ni-like Mechanism). The use of the reaction coordinate (RC = d(O3B−C1′) − d(O4−C1′)) to model the front-side attack of LAT at UDP-Gal results in a smooth energy profile with a single energy barrier of ∼12 kcal/mol at the QM(B3LYP/TZVP//BP86/SVP)/CHARMM level (see Figure 3). The changes in the distances between the reactive atoms along this reaction path (Figure 3) indicate that the computed S_Ni mechanism has a highly dissociative character: the C1′−O3B bond breaks early in the reaction, the attacking O4 atom from LAT slowly approaches C1′, and both the HO4−O3B and O4−C1′ bonds form simultaneously and concomitant with the rapid drop in energy that is observed right after the maximum in Figure 3. It should be noted that, in the reactant complex, the O3B oxygen of the phosphate leaving group is already well oriented to act as the base to deprotonate the acceptor in the S_Ni mechanism (d(HO4−O3B) = 1.67 Å). This possible role of the leaving group as the base catalyst has initially been invoked by Sinnott and Jencks[13] for the solvolysis of glycosyl fluoride by trifluoroethanol and has recently also been suggested for OtsA.[14] In the cluster model by Tvaroška, UDP was also found to accept the HO4 proton, but in the reactant state, the O3B−HO4 distance was significantly longer than in the present work (d(HO4−O3B) = 2.33 Å).[16] The distances at the energy maximum of Figure 3 are d(O3B−C1′) = 3.22 Å, d(O4−C1′) = 2.16 Å, d(O4−HO4) = 1.07 Å, and d(HO4−O3B) = 1.36 Å, clearly indicating a highly dissociative character. This rationalizes the finding that the use of a single distance (d(O4−C1′) or d(O3B−C1′)) as reaction coordinate for this chemical event did not work satisfactorily (SI, Figure S2).

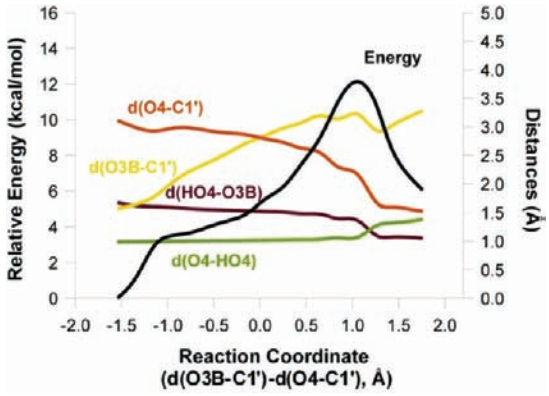

Figure 3. QM(B3LYP/TZVP//BP86/SVP)/CHARMM energy profile for the front-side attack mechanism. The variation of several interatomic distances involved in the reaction is also depicted. See Scheme 2 for a clearer picture of the reaction under study.

The structure of the energy maximum in Figure 3 was used as the starting point for a TS search (see Models and Methods). The computed energy barriers and reaction energies are given in Table 1, while key bond distances and NPA charges of reactants, TS, and products are listed in Table 2. The TS structure is shown in Figure 4. In the following discussion, we focus on single-point QM/CHARMM energies obtained with QM = M05-2X/TZVP and B3LYP/TZVP at geometries optimized with QM = BP86/SVP, which are expected to be our most reliable energy data (SI, Section 1.2). A more detailed comparison of the energies and geometries obtained at different levels is available in the Supporting Information (Section 2 and Table S2).

Table 1. QM/MM Potential Energy Barrier and Reaction Energy (in kcal/mol) for the Proposed S_Ni Mechanism at Different Levels of Theory

QM treatment	$V^{\ddagger}$	ΔV_R
BP86/SVP	9.2	3.3
BP86/TZVP//BP86/SVP	8.1	4.6
BP86/def2-TZVPP(d)//BP86/SVP	8.8	4.6
B3LYP/SVP// BP86/SVP	12.9	4.6
B3LYP/SVP	11.1	4.6
B3LYP/TZVP//BP86/SVP	11.8	6.1
B3LYP-D/TZVP//BP86/SVP	9.5	2.8
B3LYP/def2-TZVPP(d)//BP86/SVP	12.5	6.1
M05-2X/SVP//BP86/SVP	16.6	3.6
M05-2X/TZVP//BP86/SVP	14.6	4.6
SCC-DFTB	32.7	9.7
B3LYP/TZVP//SCC-DFTB	15.4	10.3
M05-2X/TZVP//SCC-DFTB	17.2	10.5

Table 2. Selected QM/CHARMM Bond Distances d (Å) and Atomic Charges q (e) in the Optimized Reactants, Transition State, and Products for the Front-Side Single Displacement Mechanism, with QM = BP86/SVP (B3LYP/SVP) for the Distances and QM = B3LYP/TZVP//BP86/SVP for the Charges

	reactant	TS	product
d(O3B−C1′)	1.57(1.53)	3.12(3.19)	3.28(3.30)
d(O4−C1′)	3.11(3.14)	2.18(2.06)	1.52(1.49)
d(O4-HO4)	0.99(0.97)	1.07(1.06)	1.38(1.44)
d(HO4−O3B)	1.67(1.71)	1.36(1.36)	1.06(1.02)
d(OE1−C1′)	3.38(3.40)	2.87(2.89)	3.05(3.09)
d(C1′−O5′)	1.36(1.36)	1.29(1.29)	1.38(1.38)
q(C1′)	0.38	0.49	0.34
q(O5′)	−0.47	−0.41	−0.50

The energy barriers obtained with M05-2X/TZVP and B3LYP/TZVP are 14.6 and 11.8 kcal/mol, respectively. Both values slightly underestimate the phenomenological free energy barrier of ∼16 kcal/mol (derived from the experimental k_{cat} values of 14−34 s^{-1} at 303 K),[11,12,61] but they do show that an

dx.doi.org/10.1021/ja210490f | J. Am. Chem. Soc. 2012, 134, 4743−4752

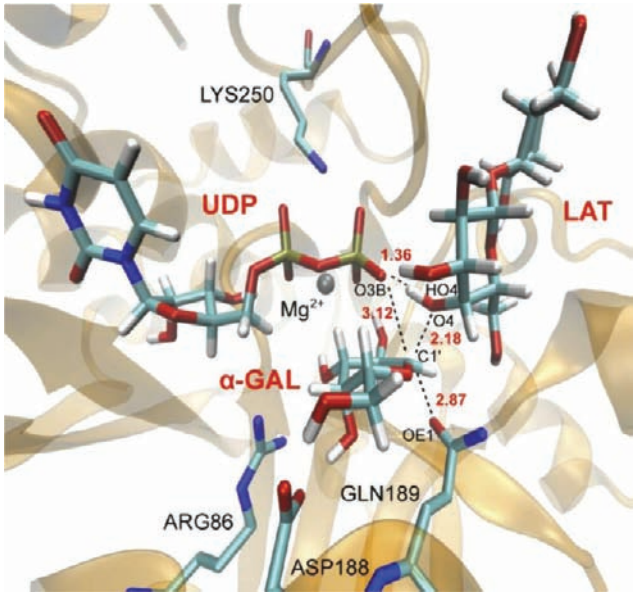

Figure 4. QM(BP86/SVP)/CHARMM optimized transition state. The donor and acceptor substrates, together with some relevant residues, are represented as sticks. Selected distances (in Å) are indicated in red.

S_Ni mechanism is plausible and consistent with the experimental data. Interestingly, the distances obtained for the optimized TS structure [d(O3B−C1′) = 3.12 Å, d(O4−C1′) = 2.18 Å, d(O4−HO4) = 1.07 Å, and d(HO4−O3B) = 1.36 Å] are very similar to those reported for the energy maximum in Figure 3, confirming that the reaction coordinate used to describe the reactive process is adequate. The sugar ring goes from the initial distorted $^4C_1$ chair (φ = 236°, θ = 9°) in the reactant complex to a conformation between an ^4E envelope and a $^4H_5$ half-chair at the TS (φ = 250°, θ = 41°). The oxocarbenium nature of the TS is also reflected in a d(C1′−O5′) distance that is slightly shorter than in the reactant (by 0.07 Å) and in the charge development during the reaction (Table 2). When going from reactant to TS, the charge of the α-Gal moiety increases by $\Delta q(\alpha\text{-Gal})$ = 0.30 e, with the main contributions coming from the ring atoms C1′ and O5′, Δq(C1′) = 0.11 e and Δq(O5′) = 0.06 e. This is accompanied by an increase in the negative charge of the UDP moiety (Δq(UDP) = −0.36 e) dominated by the large change at the leaving oxygen atom (Δq(O3B) = −0.24 e), and by a smaller change in the lactose, mainly at the attacking oxygen atom ($\Delta q(\beta\text{-Gal})$= 0.09 e, Δq(O4) = 0.05 e).

Our results for LgtC thus indicate that there is a direct one-step path connecting reactant, TS, and products, which corresponds to a highly dissociative S_Ni mechanism (Scheme 1B). This is consistent with recent experiments on another retaining GT. In one of these experiments, Davies and co-workers[14] report the crystal structure of the retaining glycosyltransferase OtsA in a complex with UDP and a bisubstrate analogue, in which the leaving-group phosphate oxygen is sufficiently close to the acceptor nucleophile (analogous to O4 in LgtC) to act as a base to deprotonate the acceptor in a front-side attack mechanism (Scheme 1B or 1C). Kinetic isotope-labeling experiments[15] further support this type of mechanism and indicate an important charge development at the anomeric center at the transition state or intermediate of the reaction. In the computational work of Tvaroška[16] on a cluster model of LgtC, an S_Ni mechanism was also suggested although some structural differences with the present study should be highlighted: the gas-phase cluster model predicts an earlier TS with shorter d(O3B−C1′) = 2.66 Å and longer d(C1′−O4) = 2.34 Å distances, and in the reactant complex, the d(C1′−O4) = 3.50 Å and d(O3B−HO4) = 2.33 Å distances are much longer than those obtained here, probably due to a different donor−acceptor orientation because of the missing enzyme environment. In the very recent computational work on OtsA,[18] which has a GT-B fold and lacks a putative nucleophile residue that could act in a double-displacement mechanism, it has been concluded that the cleavage of the α,α-1,1 linkage is catalyzed in a two-step mechanism via an extremely short-lived ion-pair intermediate (Scheme 1C, S_Ni-like mechanism).

During the front-side attack of LAT on UDP-Gal, the anomeric carbon and the OE1 atom of Gln189 (the putative nucleophile in a double displacement mechanism) get closer by ∼0.5 Å. This is mainly caused by the change in the ring puckering on the way from the reactants to the TS (see above). The decrease in the d(C1′−OE1) distance, from 3.38 to 2.87 Å, may help to stabilize the increasing positive charge at the anomeric center. Like in the cluster model,[16] Gln189 (via Nε) forms a hydrogen bond with the O6 atom of β-Gal of LAT, with d(H−O6) distances of 2.0 and 1.9 Å in the reactants and the TS, respectively. This interaction is thus involved both in the binding of LAT and in keeping the proper orientation of the substrate during the reaction. The previously reported[16] interaction between Nε (Gln189) and O5′ is not seen in our QM/MM calculations where Nε (Gln189) is permanently hydrogen bonded to the hydroxyl group of Tyr151. Again, this difference may arise from the limitations of the cluster model that does not include Tyr151.

Umbrella sampling molecular dynamics simulations at the SCC-DFTB/CHARMM22 level were used to estimate the free energy barrier of the front-side mechanism. Although this electronic structure method severely overestimates the energy barrier (Table 1), it is still expected to provide a reasonable estimate of the differences between the potential energy and free energy profiles. These and the corresponding barriers are found to be practically identical, indicating that entropic effects are minor in the reaction under study (SI, Figure S3). This is consistent with the highly dissociative character of the TS.

Double Displacement Mechanism. All attempts to locate the covalent glycosyl-enzyme complex (CGE) for the wild-type enzyme failed. The d(OE1−C1′) distance would seem to be a natural reaction coordinate for driving the reactants toward the CGE intermediate. A corresponding reaction path calculation indeed yields a CGE-type structure, with d(OE1−C1′) = 1.58 Å and d(O3B−C1′) = 3.27 Å. However, the energy profile is monotonously increasing (SI, Figure S4), and an unrestrained minimization of the last point leads back to the reactants again. Along this path, the d(O4−C1′) distance stays close to its initial value of 3.11 Å, showing just some small fluctuations (0.1 Å).

Figure 5 illustrates the different mechanistic proposals for LgtC using a two-dimensional potential energy surface (PES) diagram. At fixed values of the d(OE1−C1′) distance, the QM/MM energy was computed by constrained optimizations along the reaction coordinate RC = d(O3B−C1′) — d(O4−C1′); note that the x-axis in Figure 5 is just d(O4−C1′). Obviously, the only energy minima in Figure 5 are those for the reactants (R, top-right corner) and for the products (P, top-left corner). There is no minimum in the region of the putative intermediate

dx.doi.org/10.1021/ja210490f | J. Am. Chem. Soc. 2012, 134, 4743−4752

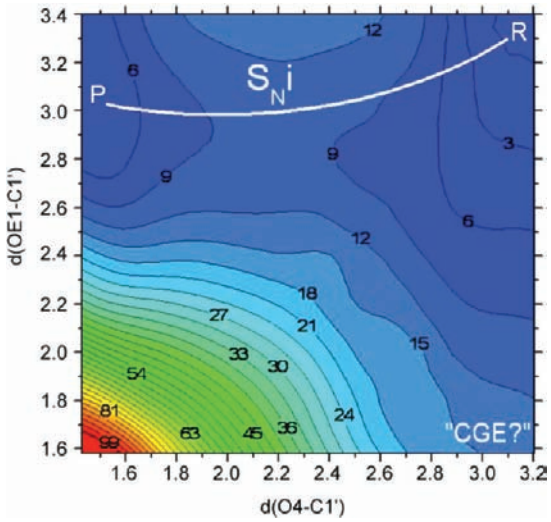

Figure 5. Two-dimensional QM(BP86/SVP)/CHARMM potential energy surface. Energies are given in kcal/mol and distances in Å. Contour lines are drawn in intervals of 3 kcal/mol.

(CGE, bottom-right corner), and hence no evidence for the proposed double-displacement mechanism in the wild-type enzyme that would require CGE formation by nucleophilic attack of Gln189. By contrast, one can easily identify a path connecting reactants and products via an oxocarbenium ion-like transition state (Figure 5). The corresponding transition state is of dissociative character and belongs to a one-step S_Ni reaction.

Test calculations with Mn^{2+} in place of Mg^{2+} have been done to ensure that the replacement used in this work is valid and does not compromise the mechanistic conclusions drawn. The potential energy profiles for both mechanisms remain essentially the same (SI, Figure S5).

Analysis of Factors Contributing to Catalysis. The QM/MM results presented so far show that the front-side attack of LAT at UDP-Gal (S_Ni mechanism) is preferred and can proceed at a reasonable energetic cost in the LgtC active site. The energies and distances computed along the S_Ni reaction path (Figure 3) show that the O3B−C1′ bond starts to break already in the initial stage of the reaction, while the d(O4−C1′) distance still remains above 2.5 Å; the QM/MM energy then reaches its maximum with the O3B−C1′ distance getting even longer and the O4 atom beginning to attack the anomeric center; finally, the energy decreases abruptly after the TS, when the O4−C1′ bond is formed and HO4 is transferred from O4 to O3B. This proton transfer seems crucial for the decrease of the energy in the final stage of this reaction. There are different factors that facilitate the reaction and contribute to the stabilization of the transition state. UDP is known to be a good leaving group, especially if coordinated to a metal cation that can stabilize the negatively charged phosphate. Moreover, it has been suggested[4] that it is because of the use of high-energy donor substrates that retaining GTs can catalyze the reaction via an a priori more expensive S_Ni type mechanism, instead of using a double-displacement mechanism as the retaining glycosidases do. The question then arises whether there are also other factors that may be helpful, for example, intrasubstrate and enzyme−substrate interactions in the TS structure (Figure 4).

Interactions between Substrates. Three hydrogen bonds between the donor and the acceptor substrates can be seen in Figure 4: one involving O4 (as well as HO4) and O3B; another one between O2′ (HO2′) and O1B (i.e., the oxygen atom of the β phosphate coordinated to the metal cation); and a third one between O3 (HO3) and O3B. All of them are present in the reactants (with O−H···O distances of 1.67, 1.68, and 1.94 Å, respectively, at the QM(BP86/SVP)/CHARMM22 level). These hydrogen bonds get shorter at the TS (1.36, 1.64, and 1.65 Å, respectively) and thereby stabilize the increasing negative charge in UDP. Another interaction that may help stabilizing the highly charged phosphate at the TS is the H-bond between O2A of the α phosphate and O3 of the UDP ribose.

To estimate the energy contribution provided by these H-bonds, we produced in silico variants of the substrates (UDP-2′-deoxygalactose and 3-deoxylactose) and calculated the front-side attack pathway for each of them at the QM(BP86/SVP)/CHARMM level using the d(O3B−C1′) — d(O4−C1′) reaction coordinate. This was followed by optimization and characterization of the corresponding transition states. The results are presented in Figure 6 (see also SI, Tables S4 and S6

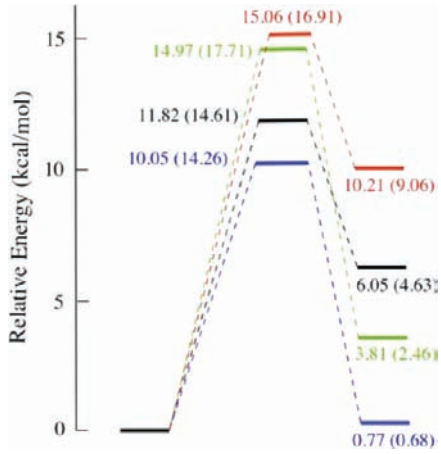

Figure 6. QM/CHARMM potential energy barriers and reaction energies for the front-side attack mechanism (S_Ni), with QM = B3LYP/TZVP//BP86/SVP (M05-2X/TZVP//BP86/SVP). Color code: black, unmodified wild-type enzyme and substrates; red, wild type with modified substrates UDP-2′-deoxygalactose and lactose; green, wild type with modified substrates UDP-Gal and 3-deoxylactose; blue, Q189A mutant with unmodified substrates.

for other levels of theory). The computed barrier heights confirm that substituting one of these OH-groups by a hydrogen atom impedes the reaction significantly: it increases the barrier by 2.3−3.3 kcal/mol compared with the unmodified substrates. Assuming that these differences are maintained in the free energy barriers, this would reduce the k_{cat} value of the mutants to 0.6−3% of that of the wild type at room temperature. The use of modified substrates leads to somewhat earlier TSs, as indicated by the optimized distances d(O3B−C1′) = 3.09/3.06 Å, d(O4−C1′) = 2.39/2.35 Å, d(O4−HO4) = 1.11/1.08 Å, and d(HO4−O3B) = 1.29/1.35 Å for the substrates UDP-2′-deoxyGal/3-deoxyLAT, respectively.

The changes in the computed TS geometries are similar for both modifications, although the replacement of the 3-OH group by H in lactose tends to increase the computed barrier slightly more. By contrast, the reaction energy is affected much more when the 2′−OH group of the α-galactose of UDP-Gal is replaced by H, leading to a rather high endoergicity of ∼9 kcal/mol. If we would substitute the 2′−OH group of UDP-Gal by

fluorine instead of hydrogen, the oxocarbenium ion-like transition state should be further destabilized inductively, and the result can easily be an inert UDP-2′FGal (which acts as a competitive inhibitor with respect to UDP-Gal), as has been observed experimentally.[12]

Enzyme–substrates Interactions; Key Enzyme Residues. The TS structure in Figure 4 also indicates several interactions between the enzyme and the substrates that may contribute to TS and/or product stabilization and thus facilitate the reaction via this mechanism. These interactions are also present in the reactants and in the crystallographic structure (Figure 1).[12] We have estimated the contribution of individual residues to the (electrostatic) stabilization/destabilization of the system by charge deletion analysis (see Models and Methods). The results for the most relevant residues are shown in Figure 7.

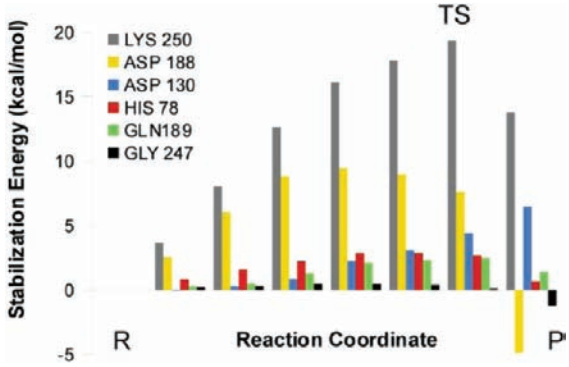

Figure 7. Electrostatic contribution to the stabilization of the QM region by selected residues surrounding the substrates. The reaction coordinate corresponds to the front-side attack mechanism [QM-(BP86/SVP)/CHARMM data].

The most prominent contribution comes from Lys250, with ∼19 kcal/mol of TS stabilization compared to the reactants. This strong effect is caused by the interaction of the charged Lys side chain with the α and β phosphates of the leaving UDP: in fact, a new H-bond involving O2B appears at the TS (H···O2B distance: 2.98 Å in the reactants and 2.18 Å in the TS). On the other hand, the H-bond between Lys250 and O2A lengthens from 1.67 Å in the reactants to 1.80 Å in the TS. Lys250 is highly conserved in the GT8 family and belongs to one of the two loops that fold over the donor substrate and are thought to be disordered in its absence;[12] hence, Lys250 is also crucial for substrate binding. The H-bond of the β phosphate (O2B) with Gly247 is very weak, while that with His78 provides a stabilization of 2.5 kcal/mol around the TS (and up to 3 kcal/mol earlier). The electrostatic interactions involving Asp188 (H-bonded to O4′ and O6′ of α-Gal) are most important (up to 9 kcal/mol) at an early stage of the reaction, while those involving Asp130 (H-bonded to O6 of β-Gal of lactose) become more prominent as the reaction proceeds (6 kcal/mol around the TS). Although some residues like Asp188 and Lys250 exhibit strong stabilization effects, their inclusion in the QM region results in negligible differences when comparing the potential energy profiles (SI, Figure S6). These results confirm that the QM/MM partition used in this work satisfactorily describes such enzyme–substrates interactions.

Gln189, the putative nucleophile in a double displacement mechanism, provides very little stabilization in the reactants, which increases up to 2.5 kcal/mol on the route to the TS, where it amounts to ∼2 kcal/mol before it drops off again (Figure 7). This stabilization mostly comes from the interaction of the anomeric center C1′ and the OE1 atom of Gln189 and is correlated with the changes in the C1′–OE1 distance (see Table 2). The transient decrease of this distance helps to stabilize the charge development at C1′ during the reaction: this charge shows a quick initial rise and then levels off before decreasing again around the TS (Figure 8).

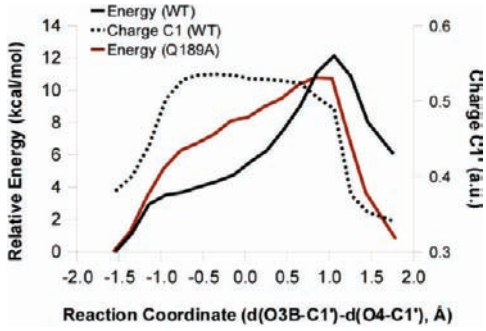

Figure 8. QM(B3LYP/TZVP)/CHARMM energy profile along the d(O3B–C1′) − d(O4–C1′) reaction coordinate at QM(BP86/SVP)/CHARMM optimized geometries, for the wild-type enzyme and the Q189A mutant. The charges at the anomeric center of the wild type enzyme were computed at the same level of theory.

Q189A Mutant. Experimentally, the Q189A mutant has its k_{cat} value reduced to 3% of that of the wild-type enzyme,[12] which translates into an increase of about 2 kcal/mol in the phenomenological free energy barrier. At first sight, this agrees well with the computed electrostatic TS stabilization due to Gln189 (see above) which will be absent in the Q189A mutant. Of course, the Q189A replacement causes other changes too, and therefore, we decided to build the Q189A mutant in silico starting from the coordinates of the wild-type enzyme and making the required substitutions for residue 189. The energy profile for the front-side attack reaction was then recalculated (see Figure 8 and SI, Figure S7), and the corresponding reactants, TS, and products were reoptimized.

Contrary to expectation, the computed QM/CHARMM energy barrier for the Q189A mutant (see Figure 6 and SI, Table S6) is slightly smaller than that for the wild-type enzyme, by 1.8 kcal/mol for QM = B3LYP/TZVP//BP86/SVP and by 0.4 kcal/mol for QM = M05-2X/TZVP//BP86/SVP. The effect of the mutation on the potential energy barrier is thus relatively small, especially for M05-2X, but still in the wrong direction.

Inspection of the computed energy profiles shows that the initial breaking of the C1′–O3B bond and approach of the attacking O4 atom is more difficult for the Q189A mutant, making its energy profile much wider and higher initially (Figure 8). However, the TS occurs somewhat earlier in the mutant compared with the wild type, and the energy thus has to rise more in the latter before the TS is reached (Figure 8). In the optimized QM(BP86/SVP)/CHARMM TS structure, the key distances are d(O3B–C1′) = 3.03 Å, d(O4–C1′) = 2.40 Å, d(O4–HO4) = 1.04 Å, and d(O3B-HO4) = 1.66 Å, that is, the breaking bond is shorter and the forming bond is longer than in the case of the wild-type enzyme. The Q189A mutant thus has an earlier TS with less dissociative character. One may speculate that this could enhance entropic effects (a tighter TS would make $\Delta S^{\ddagger}$ more negative and $\Delta G^{\ddagger}$ more positive, because of the larger $-T\Delta S^{\ddagger}$ term). We have not quantified

dx.doi.org/10.1021/ja210490f | J. Am. Chem. Soc. 2012, 134, 4743–4752

such effects, however, and therefore refrain from speculating whether this may explain the wrong trend in the computed barriers (see above).

In summary, the Q189A mutant still follows the S_Ni mechanism although with a somewhat less dissociative TS. Whether the enzyme has a single dissociative oxocarbenium ion-like TS (S_Ni) or a short-lived ion-pair intermediate (S_Ni-like) obviously depends on the actual shape of the potential (or free) energy surface along the reaction coordinate (from RC ~ −1.5 to 1.0 Å, see Figure 8), or in other words, on the extent and timing of the making and breaking of bonds.[15] The Q189A mutation with the replacement of a weak nucleophile already significantly affects the energy profile and the location of the TS (see Figure 8 and SI, Figure S7). It is conceivable that other mutations lead to larger changes, up to a point where another local minimum for an ion-pair intermediate appears. Therefore, the tuning by the environment may determine the exact mechanism followed by the enzyme (S_Ni vs S_Ni-like). We note in this connection again that the recent QM/MM work on OtsA suggests an S_Ni-like mechanism with a very shallow ion-pair intermediate.[18]

Q189E Mutant. If Gln189 assists the reaction by stabilizing the charge development at the anomeric center, the Q189E mutation would be expected to provide a much better stabilization and, thus, favor the S_Ni mechanism even more. This is exactly what we find if we transform in silico Gln189 to a pseudo-glutamate (Q189E*) by simply including this residue in the MM part of the system and giving it the charges of a glutamate, without changing the geometries obtained for the WT enzyme (SI, Figure S8). However, when we actually build the Q189E mutant in silico and perform reoptimizations (in analogy to the procedure outlined above for the Q189A mutant), another scenario emerges.

Energy minimization of the Q189E mutant takes the system straight to the CGE complex, indicating that in this case CGE formation is barrierless. At the QM(BP86/SVP)/CHARMM level, the C1′−O(Glu189) distance in the formed CGE is 1.49 Å. The interaction with the Ala154 amide is maintained, but not the hydrogen bond with the O6 atom of LAT (which is oriented to make a hydrogen bond with Asp130, Figure 9A). The S_N2 attack of LAT at the CGE, in what would be the second step of the double displacement mechanism, was studied by scanning the d(O4−C1′) reaction coordinate at different levels of theory (SI, Figure S9). In all DFT-based energy profiles, the computed barrier is higher than 30 kcal/mol. TS optimization has only been successful for SCC-DFTB/CHARMM, yielding a barrier height of 28.8 kcal/mol that increased to 33.9 and 39.5 kcal/mol in single-point energy calculations with QM = B3LYP/TZVP and M05-2X/TZVP, respectively. According to these QM/MM results, the overall reaction for the Q189E mutant would thus be very slow, and moreover, the reaction energy is also computed to be very high (26−30 kcal/mol). Key distances in the SCC-DFTB/CHARMM TS structure are d(C1′−OE1) = 2.31 Å, d(O4−C1′) = 2.19 Å, d(O4−HO4) = 1.18 Å, and d(O3B−HO4) = 1.23 Å (Figure 9B).

The case of the Q189E mutant would be an example of a change in mechanism introduced by a mutation. Recently, Goedl and Nidetzky[62] have remodeled sucrose phosphorylase to change its kinetics and chemical mechanism from a double-displacement to a direct front-side nucleophilic displacement reaction. In our calculations, we observe CGE formation in the Q189E mutant, but galactosyl transfer via a double displacement mechanism involving Glu189 has a high barrier and is thus too slow to be feasible, at least in the presently studied conformation of the enzyme. We note that O4 access to C1′ is hampered by H1′ and also limited by the need to keep the O3B−HO4 interaction. This enforces a TS structure with a dissociated C1′−OE2 bond, but in the resulting species, Glu189 does not seem to be stabilized enough by the environment. In fact, kinetic experiments on the Q189E mutant of LgtC found a reduction in k_{cat} to 3% of that of the wild-type enzyme and a reduction in its (low) hydrolytic activity by a factor of 10.[11] Formation of a CGE intermediate was indeed detected but involved Asp190, whose side chain carboxylate is located as far as 8.9 Å away from the anomeric carbon C1′ in the Q189E:UDP-2′FGal crystal structure. These experimental results suggest the possibility of a double-displacement mechanism in the Q189E mutant, in which the remote residue Asp190 acts as the catalytic nucleophile. This would obviously require significant conformational changes (relative to the wild-type crystal structure) to correctly position Asp190, which might occur as a consequence of the mutation or upon acceptor binding. A detailed understanding of the reaction in the Q189E mutant would clearly require further experimental and computational studies that are beyond the scope of the present work.

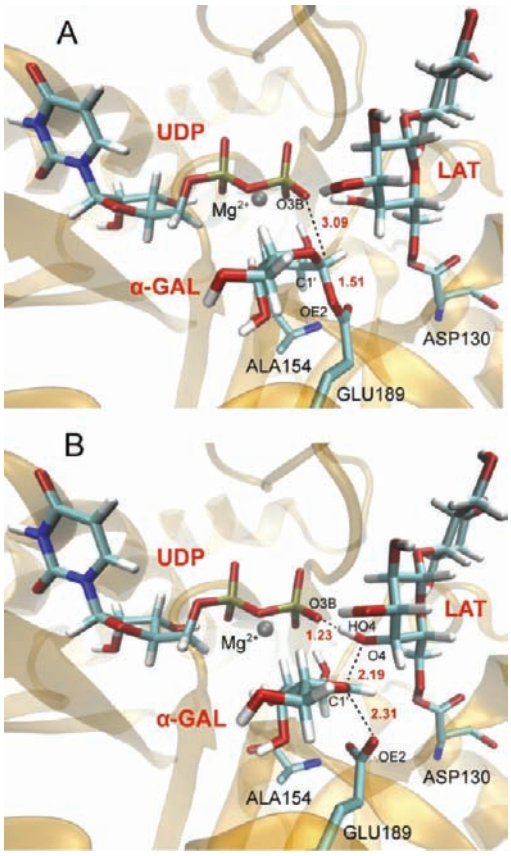

Figure 9. Optimized (A) covalent glycosyl−enzyme complex and (B) transition state for the second step of a double-displacement mechanism in the LgtC Q189E mutant optimized at the SCC-DFTB/CHARMM level. Selected distances (in Å) are indicated in red.

Further Comparisons. There are other retaining GTs which do contain a bona fide nucleophile in the active site. This is the case for the family 6 GT bovine α-1,3-galactosyltransferase (α3GalT),[63] which has a glutamate (Glu317) at the

dx.doi.org/10.1021/ja210490f | J. Am. Chem. Soc. 2012, 134, 4743−4752

position equivalent to Gln189. It has been proposed that the presence of Glu317 is required for proper acceptor-substrate orientation. α3GalT utilizes the same substrates as LgtC, namely, UDP-Gal and LAT, but catalyzes the formation of an α-1,3 glycosidic linkage. An overlay of the structures of these two enzymes (SI, Figure S10) shows that the substrates indeed adopt different relative orientations and that Glu317 and Gln189 participate in correctly orienting the acceptor. Consequently, some of the interactions identified in this work that favor the S_Ni mechanism in LgtC are not present in α3GalT, for example, the O3(LAT)−O3B(UDP) hydrogen bond. Apparently, as expected, there are connections between the identity of the substrates, the specificity of the glycosidic bond to be formed, the interactions and relative orientation of the bound substrates, and the active-site residues. And even more interestingly, all these factors could conspire to determine the mechanistic strategy followed by the enzyme. Experimental data on α3GalT and two other ret-GTs of the family 6 GTs suggest that these retaining enzymes could actually operate by a double-displacement mechanism. The second step of the double displacement mechanism for retaining α-galactosyltransferases with a glutamate nucleophile has been investigated using a cluster model and QM(DFT) calculations.[64] This study concludes that such a mechanism is plausible and that the hydroxyl group of the acceptor would attack the CGE in the second step, with the UDP acting as the general base that deprotonates the hydroxyl group. This role of UDP thus seems to be a common feature in different ret-GT mechanisms.

CONCLUSIONS

Getting a clear picture of the reaction mechanism used by retaining glycosyltransferases is very difficult experimentally and remains one of the fundamental challenges in glycosciences. Here we have used QM(DFT)/MM calculations on the full enzyme to study the reaction catalyzed by LgtC as well as the corresponding reaction with alternative substrates and with LgtC mutant enzymes. This provides us with a detailed description of the reaction catalyzed by this enzyme, which we expect will be valuable to the experimental groups working in the field. The different mechanisms proposed in the literature (S_Ni, S_Ni-like, and double displacement mechanism via the formation of a CGE intermediate) have been investigated and compared. We find a dissociative S_Ni mechanism for the wild-type enzyme with the most reliable QM/CHARMM barriers ranging between 11.8 kcal/mol (B3LYP/TZVP) and 14.6 kcal/mol (M05-2X/TZVP), in reasonable agreement with the experimental kinetic data. We have identified several factors that help the front-side mechanism, in particular enzyme−substrate and substrate−substrate interactions. Among them, the largest effects come from Lys250, which is also involved in binding. Gln189, the putative nucleophile in a double displacement mechanism, is found to favor the charge development at the anomeric center during the reaction by about 2 kcal/mol. We predict that 3-deoxylactose as acceptor will increase the barrier height by 2−3 kcal/mol (reduction of k_{cat} to 0.6−3% of that for the unmodified substrates). The reactions of the Q189A and Q189E mutants have also been investigated. Comparison of LgtC wild type and mutant systems, as well as other ret-GTs, suggest that the mechanistic strategy followed by each enzyme−substrate complex may be influenced by several factors, including the nature of the substrates, the specificity of the glycosidic linkage to be formed (and thus the interactions and relative orientation of the bound substrates), or even the GT fold. Thus, it should not be expected that all retaining GTs share the same mechanism. In OtsA, no putative nucleophile is present and an S_Ni-like mechanism was proposed; a poor nucleophile is present in wild-type LgtC, and the enzyme is found to follow a dissociative S_Ni mechanism; and when Gln189 is substituted by Ala (Q189A), an S_Ni mechanism is still predicted but with a less pronounced maximum and a wider and flatter barrier top. For the LgtC Q189E mutant, an even more drastic change in mechanism is computed, from a front-side attack to the formation of a CGE with Glu189 that cannot evolve to the products, at least not with the present enzyme conformation. Finally, ret-GTs of family 6 GTs, with a well-defined nucleophile present in the active site, seem to follow a double-displacement mechanism. Therefore, a full understanding of the mechanism used by retaining glycosyltransferases would seem to require case-by-case studies. In an attempt to shed more light on these mechanisms, other ret-GT systems are now being investigated in our laboratory.

ASSOCIATED CONTENT

Supporting Information

Computational details, QM/MM results (geometries and energies) for all methods used in each of the reactions studied, including the tests with Mn^{2+}; complete refs 23, 27, 29, and 31 (PDF); and optimized geometries of the 18 stationary points determined in this study plus the optimized reactants complex with Mn^{2+} (pdb). This material is available free of charge via the Internet at http://pubs.acs.org.

AUTHOR INFORMATION

Corresponding Author

Laura.Masgrau@uab.cat

Notes

The authors declare no competing financial interest.

ACKNOWLEDGMENTS

We acknowledge financial support from the Spanish "Ministerio de Ciencia e Innovación" through project CTQ2008-02403/BQU, the "Ramon y Cajal" program (L.M.), and from the"Generalitat de Catalunya", project 2009SGR409.

REFERENCES

(1) Taniguchi, N.; Honke, K.; Fukuda, M. *Handbook of Glycosyltransferases and Related Genes*; Springer: Tokyo, 2002.
(2) Ünligil, U.; Rini, J. M. *Curr. Opin. Struct. Biol.* **2000**, *10*, 510−517.
(3) Breton, C.; Snajdrová, L.; Jeanneau, C.; Koca, J.; Imberty, A. *Glycobiology* **2006**, *16*, 29R−37R.
(4) Lairson, L. L.; Henrissat, B.; Davies, G. J.; Withers, S. G. *Annu. Rev. Biochem.* **2008**, *77*, 521−555.
(5) Tzeng, Y. L.; Stephens, D. S. *Microbes Intect.* **2000**, *2*, 687−700.
(6) Campbell, J.; Davies, G.; Bulone, V.; Henrissat, B. *Biochem. J.* **1998**, *329* (Pt. 3), 719.
(7) Takayama, S.; Chung, S.G-; Igarashi, Y.; Ichikawa, Y.; Sepp, A.; Lechler, R. I.; Wu, J.; Hayashi, T; Siuzdak, G.; Wong, C.-H. *Bioorg. Med. Chem.* **1999**, *7*, 401−409.
(8) Davies, G. J. *Nat. Struct. Biol.* **2001**, *8*, 98−100.
(9) Monegal, A.; Planas, A. *J. Am. Chem. Soc.* **2006**, *128*, 16030−16031.
(10) Soya, N.; Fang, Y.; Palcic, M. M.; Klassen, J. S. *Glycobiology* **2011**, *21*, 547−552.
(11) Lairson, L. L.; Chiu, C. P. C; Ly, H. D.; He, S.; Wakarchuk, W. W.; Strynadka, N. C. J.; Withers, S. G. *J. Biol. Chem.* **2004**, *279*, 28339−28344.

(12) Persson, K.; Ly, H. D.; Dieckelmann, M.; Wakarchuk, W. W.; Withers, S. G.; Strynadka, N. C. *Nat. Struct. Biol.* **2001**, *8*, 166−175.
(13) Sinnott, M. L.; Jencks, W. P. *J. Am. Chem. Soc.* **1980**, *102*, 2026−2032.
(14) Errey, J. C.; Lee, S. S.; Gibson, R. P.; Martinez Fleites, C.; Barry, C. S.; Jung, P. M. J.; O'Sullivan, A. C.; Davis, B. G.; Davies, G. J. *Angew. Chem., Int. Ed.* **2010**, *49*, 1234−1237.
(15) Lee, S. S.; Hong, S. Y.; Errey, J. C.; Izume, A.; Davies, G. J.; Davis, B. G. *Nat. Chem. Biol.* **2011**, *7*, 631−638.
(16) Tvaroška, I. *Carbohydr. Res.* **2004**, *339*, 1007−1014.
(17) Wallace, A. C.; Laskowski, R. A.; Thornton, J. M. *Protein Eng.* **1995**, *8*, 127−134.
(18) Ardèvol, A.; Rovira, C. *Angew. Chem., Int. Ed.* **2011**, *50*, 10897−10901.
(19) Li, H.; Robertson, A. D.; Jensen, J. H. *Proteins* **2005**, *61*, 704−721.
(20) Fraústo da Silva, J. J. R.; Williams, R. J. P. *The Biological Chemistry of Elements. The Inorganic Chemistry of Life*; Clarendon Press: Oxford, England, 1991.
(21) Bock, C. W.; Katz, A. K.; Markham, G. D.; Glusker, J. P. *J. Am. Chem. Soc.* **1999**, *121*, 7360−7372.
(22) Kóňa, J.; Tvaroška, I. *Chem. Pap.* **2009**, *63*, 598−607.
(23) MacKerell, A. D. Jr.; et al. *J. Phys. Chem. B* **1998**, *102*, 3586−3616.
(24) MacKerell, A. D., Jr.; Brooks, C., III; Nilsson, L.; Roux, B.; Won, Y.; Karplus, M. In *The Encyclopedia of Computational Chemistry*; Schleyer, P. v. R., Ed.; John Wiley & Sons: Chichester, 1998; pp 271−277.
(25) MacKerell, A. D. Jr.; Feig, M.; Brooks, C. L. *J. Am. Chem. Soc.* **2004**, *126*, 698−699.
(26) Brooks, B. R.; Bruccoleri, R.; Olafson, D.; States, D.; Swaminathan, S.; Karplus, M. *J. Comput. Chem.* **1983**, *4*, 187−217.
(27) Brooks, B. R.; et al. *J. Comput. Chem.* **2009**, *30*, 1545−1614.
(28) Guvench, O.; Hatcher, E. R.; Venable, R. M.; Pastor, R. W.; MacKerell, A. D. Jr. *J. Chem. Theory Comput.* **2009**, *5*, 2353−2370.
(29) Sherwood, P.; et al. *J. Mol. Struct. (THEOCHEM)* **2003**, *632*, 1−28.
(30) Ahlrichs, R.; Bär, M.; Häser, M.; Horn, H.; Kölmel, C. *Chem. Phys. Lett.* **1989**, *162*, 165−169.
(31) Frisch, M. J.; et al. *Gaussian03*, revision D.01; Gaussian, Inc.: Wallingford, CT, 2004.
(32) Thiel, W. *Program MNDO2005*, version 7.0; Max-Planck-Institut für Kohlenforschung: Mülheim, 2005.
(33) Slater, J. C. *Phys. Rev.* **1951**, *81*, 385−390.
(34) Vosko, S. H.; Wilk, L.; Nusair, M. *Can. J. Phys.* **1980**, *58*, 1200−1211.
(35) Becke, A. D. *Phys. Rev. A* **1988**, *38*, 3098−3100.
(36) Perdew, J. P. *Phys. Rev. B* **1986**, *33*, 8822−8824.
(37) Perdew, J. P. *Phys. Rev. B* **1986**, *34*, 7406.
(38) Becke, A. D. *J. Chem. Phys.* **1993**, *98*, 5648−5652.
(39) Stephens, P. J.; Devlin, F. J.; Chabalowski, C. F.; Frisch, M. J. *J. Phys. Chem.* **1994**, *98*, 11623−11627.
(40) Lee, C. T.; Yang, W. T.; Parr, R. G. *Phys. Rev. B* **1988**, *37*, 785−789.
(41) Zhao, Y.; Schultz, N. E.; Truhlar, D. G. *J. Chem. Theory Comput.* **2006**, *2*, 364−382.
(42) Elstner, M.; Porezag, D.; Jungnickel, G.; Elsner, J.; Haugk, M.; Frauenheim, T.; Suhai, S.; Seifert, G. *Phys. Rev. B* **1998**, *58*, 7260−7268.
(43) Frauenheim, T.; Seifert, G.; Elstner, M.; Niehaus, T.; Köhler, C.; Amkreutz, M.; Sternberg, M.; Hajnal, Z.; Carlo, A. D.; Suhai, S. *J. Phys.: Condens. Matter* **2002**, *14*, 3015−3047.
(44) Smith, W. *J. Mol. Graphics* **1996**, *14*, 136−141.
(45) Bakowies, D.; Thiel, W. *J. Phys. Chem.* **1996**, *100*, 10580−10594.
(46) de Vries, A. H.; Sherwood, P.; Collins, S. J.; Rigby, A. M.; Rigutto, M.; Kramer, G. J. *J. Phys. Chem. B* **1999**, *103*, 6133−6141.
(47) Sherwood, P.; de Vires, A.; Collins, S.; Greatbanks, S.; Burton, N.; Vincent, M.; Hillier, I. *Faraday Discuss.* **1997**, *106*, 79−92.
(48) Nocedal, J. *Math. Comp.* **1980**, *35*, 773−782.
(49) Liu, D.; Nocedal, J. *Math. Programming* **1989**, *45*, 503−528.
(50) Banerjee, A.; Adams, N.; Simons, J.; Shepard, R. *J. Phys. Chem.* **1985**, *89*, 52−57.
(51) Baker, J. *J. Comput. Chem.* **1986**, *7*, 385−395.
(52) Billeter, S. R.; Turner, A. J.; Thiel, W. *Phys. Chem. Chem. Phys.* **2000**, *2*, 2177−2186.
(53) Schäfer, A.; Horn, H.; Ahlrichs, R. *J. Chem. Phys.* **1992**, *97*, 2571−2577.
(54) Eichkorn, K.; Weigend, F.; Treutler, O.; Ahlrichs, R. *Theor. Chem. Acc.* **1997**, *97*, 119−124.
(55) Eichkorn, K.; Treutler, O.; Ohm, H.; Häser, M.; Ahlrichs, R. *Chem. Phys. Lett.* **1995**, *240*, 283−289.
(56) Grimme, S. *J. Comput. Chem.* **2006**, *27*, 1787−1799.
(57) Schäfer, A.; Huber, C.; Ahlrichs, R. *J. Chem. Phys.* **1994**, *100*, 5829−5835.
(58) Rappoport, D.; Furche, F. *J. Chem. Phys.* **2010**, *133*, 134105.
(59) Reed, A. E.; Weinstock, R. B.; Weinhold, F. *J. Chem. Phys.* **1985**, *83*, 735−746.
(60) Humphrey, W.; Dalke, A.; Schulten, K. *J. Mol. Graphics* **1996**, *14*, 33−38.
(61) Ly, H. D.; Lougheed, B.; Wakarchuk, W. W.; Withers, S. G. *Biochemistry* **2002**, *41*, 5075−5085.
(62) Goedl, C.; Nidetzky, B. *ChemBioChem* **2009**, *10*, 2333−2337.
(63) Boix, E.; Swaminathan, G. J.; Zhang, Y.; Natesh, R.; Brew, K.; Acharya, K. R. *J. Biol. Chem.* **2001**, *276*, 48608−48614.
(64) André, I.; Tvaroška, I.; Carver, J. P. *Carbohydr. Res.* **2003**, *338*, 865−877.